Journal of Controlled Release 309 (2019) 94–105

Contents lists available at ScienceDirect

Journal of Controlled Release

journal homepage: www.elsevier.com/locate/jconrel

Shape effect in active targeting of nanoparticles to inflamed cerebral endothelium under static and flow conditions

A. Da Silva-Candal[a,*], T. Brown[b], V. Krishnan[b], I. Lopez-Loureiro[a], P. Ávila-Gómez[a], A. Pusuluri[b], A. Pérez-Díaz[c], C. Correa-Paz[a], P. Hervella[a], J. Castillo[a], S. Mitragotri[b,*], F. Campos[a,*]

[a] Clinical Neurosciences Research Laboratory, Clinical University Hospital, Health Research Institute of Santiago de Compostela, Santiago de Compostela, Spain
[b] John A. Paulson School of Engineering and Applied Sciences Wyss Institute, Harvard University, Cambridge, MA, 02138, United States of America
[c] Drug Screening Platform/Biofarma Research Group, Molecular Medicine and Chronic Diseases Research Center, University of Santiago de Compostela, Santiago de Compostela, Spain

ARTICLE INFO

Keywords:
Active targeting
Brain
Inflammation
Shape

ABSTRACT

Endothelial cells represent the first biological barrier for compounds, including nanoparticles, administered *via* the intravascular route. In the case of ischemic stroke and other vascular diseases, the endothelium over-expresses specific markers, which can be used as molecular targets to facilitate drug delivery and imaging. However, targeting these markers can be quite challenging due to the presence of blood flow and the associated hydrodynamic forces, reducing the likelihood of adhesion to the vessel wall. To overcome these challenges, various parameters including size, shape, charge or ligand coating have been explored to increase the targeting efficiency. Geometric shape can modulate nanoparticle binding to the cell, especially by counteracting part of the hydrodynamic forces of the bloodstream encountered by the classical spherical shape. In this study, the binding affinity of polystyrene nanoparticles with two different shapes, spherical and rod-shaped, were compared. First, vascular adhesion molecule-1 (VCAM-1) was evaluated as a vascular target of inflammation, induced by lipopolysaccharide (LPS) stimulation. To evaluate the effect of nanoparticle shape on particle adhesion, nanoparticles were coated with anti-VCAM-1 and tested under static conditions in cell culture dishes coated with cerebral microvasculature cells (bEnd.3) and under dynamic flow conditions in microfluidic channels lined with hCMEC/D3 cells. Effect of particle shape on accumulation was also assessed in two *in vivo* models including systemic inflammation and local brain inflammation. The elongated rod-shaped particles demonstrated greater binding ability *in vitro*, reaching a 2.5-fold increase in the accumulation for static cultures and 1.5-fold for flow conditions. Anti-VCAM-1 coated rods exhibited a 3.5-fold increase in the brain accumulation compared to control rods. These results suggest shape offers a useful parameter in future design of drug delivery nanosystems or contrast agents for neurovascular pathologies.

1. Introduction

Intravenous (i.v.) administration is one of the most common clinical routes for administering drugs, allowing for their rapid distribution throughout the body. However, this form of administration can lead to non-specific, often toxic, off-target effects and can require the use of high drug doses to achieve the therapeutic effect [1,2]. The possibility of encapsulating pharmaceuticals within carriers has made nanomedicine a promising approach for treating several diseases by localizing the drug at the therapeutic site.

Vascular endothelium has been widely explored as a therapeutic target of nanoparticles, primarily for inflammatory pathologies [3,4]. In response to local pro-inflammatory stimuli, the endothelial expression of cell adhesion molecules is upregulated to mediate interactions with immunological cells [5]. This allows for leukocyte adhesion to the endothelium, followed by extravasation at the site of inflammation [5]. The specific upregulation of inflammatory-mediated vascular proteins (e.g; ICAM-1 and VCAM1) has been used for targeting not only drug carriers [6,7], but also imaging agents [8].

Important physical parameters that can affect the success of nanoparticles in reaching their target in the vascular endothelium include blood flow rate and vessel tortuosity. Several aspects can be modified during the design of a nanoparticle that can improve the binding rate after *in vivo* administration, such as size, shape, and charge. The ideal

* Corresponding authors.
E-mail addresses: andres.alexander.da.silva.candal@sergas.es (A. Da Silva-Candal), mitragotri@seas.harvard.edu (S. Mitragotri), francisco.campos.perez@sergas.es (F. Campos).

https://doi.org/10.1016/j.jconrel.2019.07.026
Received 14 May 2019; Received in revised form 16 July 2019; Accepted 18 July 2019
Available online 19 July 2019
0168-3659/ © 2019 The Authors. Published by Elsevier B.V. This is an open access article under the CC BY license (http://creativecommons.org/licenses/BY/4.0/).

combination of these factors can determine the success of the binding to the cellular target [9]. Overall, particle geometry is a key parameter for vascular targeting [10]. Specifically, rod shaped particles have shown significant improvements over spherical particles [11]. The influence of shape on the binding affinity of nanoparticles with vascular endothelial cells has been studies through experimental and theoretical analyses [9,12,13]. These studies have identified several key variables including hydrodynamic forces, distance between nanoparticle and target-protein, target-protein density, and the contact area between the nanoparticle and the cell [14]. Rod-shaped particles have been particularly thought to benefit *via* improved contact area with the target compared to spherical nanoparticles [15]. In this work, we analyze the effect of nanoparticle shape when targeted to inflammatory vascular markers *in vitro* under static and dynamic flow conditions along with *in vivo* dynamic conditions.

2. Materials and methods

2.1. Preparation of rod-shaped nanoparticles

Rod-shaped particles were prepared using the film stretching method as described in previous reports using commercially-available spherical Fluoresbrite® Yellow-Orange Carboxylate polystyrene particles of 200 nm in diameter (Polysciences, PA, USA) [16]. Polyvinyl alcohol (PVA) films were first made by dissolving 5 g of PVA-hot water-soluble grade (Sigma-Aldrich, MO, USA) in 80 mL of water at 130 °C with constant stirring. Glycerol (1 mL) (Sigma-Aldrich, MO, USA) was added as a plasticizer. The PVA-glycerol solution was allowed to cool to room temperature before adding the particles. The mixture was cast on a flat surface (25cm^2) and allowed to solidify overnight. Formed films were cut and clamped in a proprietary stretching apparatus before being placed in a heated oil bath (120 °C) for 5 min. The film was then stretched to the desired dimensions for two-aspect ratio particles. Stretched particle-embedded films were dissolved in water overnight and purified by centrifugation. Particle morphology was characterized with a FEI XL30 Sirion FEG SEM Scanning electron microscopy (SEM).

For particle functionalization, 1 mg of each particle shape was diluted in 1 mL 0.5 mM of 2-(N-morpholino) ethanesulfonic acid (MES) buffer to a pH 4.7 and the same mass (1 mg) of N-(3-Dimethylaminopropyl)-N-ethylcarbodiimide (EDC) and N-Hydroxysuccinimide (NHS) was added to the mixture an activated for 15 min, then 0.5 mg of 3 K length polyethyleneglycol with a terminal azide group (NH_2-PEG-N_3) was added and allowed to react (all products Sigma-Aldrich, MO, USA). For PEG quantification experiments 0.5 mg of fluorescent PEG (NH_2-PEG-FITC) were used instead (Nanocs, Ny, USA). Two different antibodies were coupled to the nanoparticles regarding the group, anti-VCAM-1 antibody for targeted particles, and a non-specific IgG antibody for the vehicle group. For this, 50 μg of antibody was added to PBS to a concentration of 6.7 μM, then added 20 mM sodium periodate ($NaIO_4$) (Sigma-Aldrich, USA) for 45 min. The oxidation was stopped by adding ethylene glycol (Sigma-Aldrich, USA) followed by PBS washing in 3 kDa-pore filters (Amicon Ultra 3 k, Merck, USA). A 10× (with respect to the antibody molarity) amine DBCO solution was added and allowed to react for 24 h at room temperature. The non-reacted DBCO was removed by filtration. Finally, the antibody-DBCO solution was added to 1 mg of pegylated particles and allowed to react for 24 h at room temperature. Particle's zeta potential was measured by means of dynamic light scattering (Zetasizer Nano ZS, Malvern Panalytical, MA, USA).

For *in vivo* biodistribution the particles were coated with a tritiated glycine molecule (Glycine, [2 − 3H]-, 1 mCi-37 MBq, Perkinelmer, USA) prior to pegylation. The coupling was performed through and EDC/NHS reaction (same ratios and times as described above). Nanoparticle suspension was brought to a pH of 9.7 and 4 μL of ^{3}H-Glycine (1mC/mL) was immediately added. It was kept in agitation at room temperature for 24 h and it was washed by centrifugation at 21,000 ×*g* at room temperature until the supernatants obtained had no radiation present.

2.2. Experimental animals

The experimental protocols were approved by the University Clinical Hospital of Santiago de Compostela Animal Care Committee, according to the European Union (EU) rules (86/609/ CEE, 2003/65/CE, and 2010/63/EU) and as per the ARRIVE guidelines. Male Swiss mice weighing 30 g were used for this study. Mice were provided *ad libitum* access to food and water. Anesthesia was induced with sevoflurane (5–6% for induction and 3–4% for maintenance) evaporated in an oxygen–air mixture (30%:70%). Throughout the surgical period, rectal temperature was maintained at 37 ± 0.5 °C by means of an electronic thermostat-controlled warming blanket. Body temperature was maintained until animals completely recovered from anesthesia and displayed normal motor activity.

2.3. Experimental design

To evaluate the shape effect on binding affinity of nanoparticles, a total of four groups were tested: i) spheres coated with anti-VCAM-1 (targeted spheres) ii) spheres coated with a non-specific IgG antibody (vehicle spheres), iii) rods coated with anti-VCAM-1 (targeted rods) and iv) rods coated with a non-specific IgG (vehicle rods). The four nanoparticle groups were tested in four different experimental conditions: i) static *in vitro* cell culture, ii) *in vitro* flow conditions, iii) *in vivo* systemic inflamed mice and iv) *in vivo* intracerebrally inflamed mice.

2.4. Static in vitro cell culture nanoparticle accumulation

BEnd.3 microvasculature brain endothelial cells (ATCC, VA, USA) were cultured in Dulbecco's Modified Eagle Medium (DMEM), with 10% (v/v) of fetal bovine serum (FBS) and 0.1% (v/v) of penicillin-streptomycin, expanded in T75 flask (Corning, NY, USA), and incubated at 37 °C with a humidified atmosphere containing 95% air and 5% of CO_2. Media was replaced every 3 days until 80% of confluence was reached. Then, cells were detached with of 0.25% trypsin-EDTA (Gibco-Invitrogen, MA, USA), trypsin was blocked with 6 mL of complete medium (with FBS) and centrifuged for 5 min at 200 ×*g*. The pellet formed was resuspended in phosphate buffered saline (PBS) and centrifuged again. Cells were then seeded in 24-well plates and incubated under the same conditions until reaching the 80% of confluence to perform the subsequent experiments.

2.4.1. Cell inflammation induction

Inflammation induction in bEnd.3 (mouse) and hCMEC/d3 (human) endothelial cell cultures was performed using LPS of *E. coli* (O111:B4, Sigma-Aldrich, MO, USA) over a period of 6 h at a concentration of 1 μg/mL. Analysis of VCAM-1 and ICAM-1 expression was determined by immunohistology and flow cytometry to test the LPS-mediated inflammation effect.

2.4.2. Cell histological analysis

Cells were incubated with Paraformaldehyde (PFA) 4% (Sigma-Aldrich, MO, USA) for 10 min. Then incubated with a solution of PBS with 0.01% (*v*/v) Tween 20 (PBS-T), 1:200 anti-VCAM-1 monoclonal antibody (Biolegend, CA, USA) and a 5% (v/v) of donkey serum (Sigma-Aldrich, MO, USA) for 24 h at 4 °C. The unbound antibody was removed with 3 washes with PBS. Then, cells were incubated with a solution of PBS-T a 1:400 Alexa Fluor®anti-rat 594 secondary antibody (Thermo-Fischer, MA, USA) with 5% of donkey serum for 2 h at 4 °C. Cells were washed again and incubated with a solution of PBS-T and 1:6,000 Hoechst (Invitrogen, CA, USA) for 5 min at room temperature for nuclear staining and washed again. Aqua Polymount (Polysciences, CA, USA) was added to each well and kept in the dark at room temperature

for 2 h until it dried up. Samples were stored at 4 °C until imaging. The staining process was also performed in 4 control wells without LPS. Finally, cells were then imaged using an Olympus Fluoview 1000 Spectral Confocal (Olympus, Tokyo, Japan). Images of control and sample wells were acquired using the same parameters.

2.4.3. Flow cytometry analysis

Cells were detached from each flask by using a non-enzymatic dissociation buffer following manufacturer instructions (Accumax, Thermo-Fischer, MA, USA). The use of trypsin-based methods was avoided when cells were immediately tested afterwards due to the possibility of rupture of membrane proteins such as VCAM-1 and ICAM-1 compromising the antibody-target recognition. The cell suspension of each flask was counted centrifuged (100 $\times g$ for 5 min) and adjusted to 1×10^6 cells/mL in an Eppendorf tube to a final volume of 200 μL with cold PBS-T. A total of 2 μg (10 μg/mL) of anti-VCAM-1 FITC monoclonal antibody (Thermo-Fisher, MA, USA) were added to the VCAM-1 analysis group and 2 μg (10 μg/mL) ICAM-1 monoclonal Antibody Alexa Fluor® 647 (Thermo-Fisher, MA, US) for the ICAM-1 analysis group to the cell suspensions.

Once VCAM-1 and ICAM-1 expression was tested, endothelial cells were incubated with nanoparticles at three different times: 1, 3 and 6 h. Cells were then washed with PBS three times in order to remove non-internalized particles. Cells were then lysed with RIPA cell lysis buffer (Sigma-Aldrich, MO, USA), and the fluorescence of each well was measured (Ex. 530 nm, Em. 546 nm) in a Tecan Spark 10 M Multimode Plate Reader (TECAN, ZSG, Switzerland). Absolute levels of fluorescence intensity cannot be compared between spheres and rods due to the fluorophore bleaching during the rod stretching process. For this purpose, data was normalized to 100% of the added dose. Wells without particle washing (for each group) were used as positive controls and considered as 100% of uptake. A control group without particles added was used as a negative control to evaluate the cell background.

2.5. In vitro flow conditions nanoparticles accumulation

2.5.1. Microfluidic device architecture

Linear channel microfluidic devices (Cat # 101002) used in this study were obtained from SynVivo, Inc. (Huntsville, AL). Each device consisted of three linear 250 μm (width) and 100 μm (depth) channels. Each channel was lined with brain endothelial cells and experienced perfusion similar to physiological fluid flow conditions.

2.5.2. Cell culture

The immortalized human cerebral microvascular endothelial cell line (hCMEC/D3) was obtained from Millipore Sigma and maintained with EndoGRO-MV Complete Culture Media Kit supplemented with 1 ng/mL human animal-free basic fibroblast growth factor (bFGF-AF) and 1% Penicillin-Streptomycin. Cells were cultured on collagen-coated tissue culture flasks coated with 1:20 dilution of Corning® Collagen Type I, Rat Tail, which was allowed to coat in the incubator for 1 h prior to use. Cells were incubated at 37 °C, 95% humidity and 5% CO_2 until confluent. Cells were used between passage 27 and 36. For hCMEC/D3 culture microfluidic straight channels, human fibronectin (300 μg/mL) was injected into each channel and allowed to incubate for 1 h at 37 °C and 5% CO_2. Channels were perfused with complete cell culture media. To devoid the device from residual entrapped air, the device was primed using inert N_2 gas at 6 PSI for 30 min. Devices were placed inside a cell culture incubator prior to use. hCMEC/D3 grown to 70 to 80% confluency were trypsinized and resuspended in cell culture media with increased serum concentration (10%). Cell suspension at 5×10^7 cells/mL was injected into the outer compartment at 6 μL/mL using a Harvard Apparatus Pump 11 Pico Plus Elite and placed inside the incubator upside down to facilitate attachment to the upper PDMS regions of the channel. After sufficient cellular attachment, an identically seeded flask of hCMEC/D3 cells was trypsinized, and cells were seeded with the device in the upright position. Following cellular attachment, channels were perfused with complete cell culture media at 5 μL/min. Cells were fed daily by perfusion of the device with cell culture media containing 10% FBS for the first day after seeding, and 5% FBS media for each subsequent day.

To condition cells to physiological shear stresses, 5% FBS containing media was injected according to a linear ramp profile (100 nL/min to 2.35 μL/min) over 12 h using a Harvard Apparatus PHD ULTRA™ with a 6 × 10 MultiRack attachment for multi-syringe perfusion. Constant 2.35 μL/min injection rate was maintained for at least 4 h. To induce an inflammatory response, lipopolysaccharide (LPS) (1 μg/mL) was immediately injected at a constant rate of 2.35 μL/min for 6 h prior to use. Devices were inspected for any bubble formation and immediately used for further studies.

2.5.3. Nanoparticle adhesion under flow

Once straight channel devices have been inflamed using LPS, 1-mL syringes were loaded with the corresponding nanoparticle condition. Nanoparticle solutions (5E10 NP/mL) were injected at 2.35 μL/min (1.00 dyn/cm^2) for 1 h. Channels were then perfused with DPBS before and after being fixed with 4% PFA for 15 min at room temperature. Channels were imaged immediately using an Olympus Fluoview 1000 spectral confocal microscope to assess particle adhesion throughout the channels. Relative particle intensities were analyzed and assessed using ImageJ.

2.6. In vivo nanoparticle biodistribution after systemic inflammation induction

To induce systemic inflammation, 30 g Swiss male mice of were treated (i.v.) with LPS (100 μg/animal) [17–19] administered through the jugular vein. Six hours after LPS treatment, systemic inflammation was determined by mean IL-6 serum levels as a marker of inflammation [20]. Once the LPS-mediated inflammation effect was confirmed (6 h later), animals were treated i.v. through the jugular vein with tritium labelled nanoparticles (15 mg/kg, $n = 4$ animals/group). The animal control group was treated with vehicle (n = 4). Six hours later, the animals were perfused with 20 mL of cold PBS, and brain, liver, spleen, kidneys and lungs were removed, weighed, and homogenized by ultrasonication. A total of 50 μL of homogenized organ were pipetted into two detection tubes (Kartell™ vials, PerkinElemer), 12 mL of Supermix OptiPhase detection cocktail (PerkinElmer, MA, USA) was added to each tube, shaken until forming a homogeneous suspension, and immediately measured the disintegrations per minute (DPM) in a scintillation detector (Beckman Coulter LS6500 Liquid Scintillation Counter). Prior to the sample measurement, the organs of 3 healthy animals were measured without any radiation administration to evaluate the background produced. After analyzing the subsequent samples of the study, the background corresponding to each organ was subtracted.

2.7. In vivo nanoparticle biodistribution after intracerebral inflammation induction

To induce local inflammation in brain, LPS was administered in the area of the striatum region [21,22]. A dose of LPS 10 μg/animal was used in a volume of 4 μL. Systemic IL-6 serum levels were analyzed to confirm that LPS was not causing systemic effect. Six hours after intracerebral LPS injection, the animal brain was removed for subsequent histological analysis.

2.7.1. Interleukin-6 (IL-6) analysis

Mice blood was extracted from the jugular vein, centrifuged at 1,700 $\times g$, and serum was collected. To confirm the systemic inflammation LPS-response, the serum levels of IL-6 were analyzed 6 h after the induction (the maximum time point used in *in vitro* experiments). In order to confirm that local LPS injection restricted the

inflammation to the brain, IL-6 levels were analyzed in serum at 6 h and 24 h, by means of an IL-6 ELISA detection kit (LSbio, WA, USA).

2.7.2. Brain vessel immunostaining

Animals subjected to inflammatory induction were sacrificed 6 or 24 h after the stimulation (treated with either LPS 10 μg/animal or saline). After follow-up period, the animals were transcardially perfused with 20 mL of cold PBS. The brain was removed and quickly cryopreserved into 10 mL of isopentane (Merck, MA, USA) at −40 °C was embedded in OCT resin (Tissue-Tek, Japan). For histological analysis, brain samples were sectioned in 12 μm thickness slices in a cryostat (Tissue-Tek, Japan). The slides were washed with PBS for 15 min thrice and incubated during 24 h with monoclonal anti-VCAM-1 1:200 (Biolegend, CA, USA) and anti-CD31 1:200 (Abcam, Cambridge, UK) used as endothelial cell marker. After incubation, tissue samples were washed (3×) with PBS and incubated again with a solution of PBS-T and anti-rat 594 secondary antibody 1:400 (Thermo-Fischer, USA), 488 Dylight Goat anti-Rabbit (Vector, CA, USA) with 5% (v/v) of donkey and goat serum for 2 h at room temperature. Finally, slides where washed again and incubated with Hoechst (Invitrogen, USA) for nucleus staining. Microphotographs were taken using a Leica DMI 6000 B microscope with the LAS AF 1.0.0 software (Leica Microsystems, Sweden).

2.7.3. qPCR of VCAM-1 in inflamed brain

For VCAM-1 qPCR analysis, the hemisphere where LPS was injected was extracted and preserved at −80 °C. Then RNA extraction was performed using a commercial column-based method (PureLinkTM RNA Mini Kit, Invitrogen, USA) following manufacturer indications. Reverse transcription mix was composed by 4 μL of reaction buffer (five times), 2 μL of $MgCl_2$ (2.5 mM in the final volume), 1 μL of dNTPs (0.5 mM of each nucleotide in the final volume), and 1 μL of GoScript™ reverse transcriptase. The final reaction mix containing a total volume of 20 μL was incubated 5 min at 25 °C allowing annealing, and 60 min at 42 °C allowing to extend the cDNA strand. After reverse transcription, the product was diluted 1:5 in RNAse free water. Once concluded the expression of VCAM was determined by q-PCR using β-Actin as a control gene expression by means of GoTaq® qPCR masterMix (Promega, WI, USA) and Mx3005P qPCR system (Agilent technologies, CA, USA).

2.7.4. Statistical analysis

All data are presented as the mean and SD of the mean (mean ± SD). The data were first examined to assess the distribution using the D'Agostino and Pearson omnibus normality test. One-way or 2-way analysis of variance (ANOVA) followed by *post hoc* Bonferroni evaluation was used to detect significant differences between the groups. Statistical significance was set at $p < .05$. Animals were randomly assigned to treatment groups, and researchers were blinded to treatment administration, to treatments during particle accumulation assessment, and during the analysis.

3. Results

3.1. In vitro and in vivo analysis of VCAM-1 and ICAM-1 expression mediated by LPS

Immunological analysis showed that cells treated with LPS had increased expression of VCAM-1 and ICAM-1 compared with control groups (Fig. 1A) as well as by flow cytometry (Fig. 1B). Intensity expression ratio between cells stimulated with LPS and non-stimulated cells (Fig. 1 C) reflected a 4.5-fold increase in the expression of ICAM-1, whereas in the VCAM-1 group the ratio resulted in a 10-fold increase. Based on these results, VCAM-1 protein was selected as the target for the nanoparticles used in the *in vitro* and *in vivo* experiments. Overexpression of VCAM-1 observed in previous *in vitro* experiments was confirmed when experimental animals were treated i.v. with LPS 100 μg/animal as showed in the Fig. 2A by an immune-staining of VCAM-1 6 h after inflammation induction. An increase of IL-6 serum levels (Fig. 2B) confirmed the inflammatory response on VCAM-1 induced by LPS treatment.

In order to induce a selective overexpression of VCAM-1 in brain without causing a systemic inflammation in the whole animal body, LPS was stereotaxically administered in the brain parenchyma. Inmunohistological (Fig. 2A) and qPCR (Fig. 2C) analysis confirmed the local expression of VCAM-1 in the brain region stimulated by LPS. Co-localization of VCAM-1 and CD31 demonstrate the overexpression of VCAM-1 was restricted to the vascular cells. Higher expression of VCAM-1 was observed at 24 h after LPS injection. No significant blood IL-6 release was observed with intracerebral LPS injection, confirming inflammation was localized in the brain (Fig. 2B).

3.2. Nanoparticle design and functionalization

Once VCAM-1 was selected as the vascular target for both the *in vitro* and *in vivo model*, fluorescent polystyrene spherical nanoparticles of around 200 nm of diameter were stretched to rods with an aspect ratio (AR) of 2. The stretching process was confirmed by SEM (Fig. 3 A and B). Spheres surface of particles was 1.03×10^5 nm^2, while for rods was 1.22×10^5 nm^2, which represented an increase of 19.12% in the surface area in rods respect to the spheres. To optimize the nanoparticle functionalization, first a NH_2-PEG-N_3 (3.5 K) was incorporated to the nanoparticle and N-(3-Dimetilaminopropil)-N′-etilcarbodiimida/N-Hydroxysuccinimide (EDC/NHS) reaction. A fluorescent PEG with a terminal FITC group was first used to evaluate the percentage of PEG incorporated to the particles. Around 20% of the total PEG was coupled to the particles, we observed the same amount of PEG in both particles (Fig. 3C), ensuring a full coverage of the surface as confirmed by *Z*-potential. (Fig. 3F).

The antibody bioconjugation was performed on the azide groups of the pegylated nanoparticles, this required first, to incorporate a Dibenzocyclooctyne-amine (DBCO) molecule into the antibody. For this reaction, the structure of the antibody was modified by means of an oxidation with sodium periodate in the carbohydrate residues of the constant region that generated aldehyde groups that reacted with of a DBCO-amine molecule forming an imine bond. Once the antibody structure was modified, the DBCO reacted with the azide groups of the particles in a copper-free click reaction, binding covalently. The amount of antibody (anti-VCAM-1 and control non-specific IgG form) coupled to the particle was quantified my means of a Micro BCA assay (Fig. 3D). The density of antibody corrected for area showed similar binning both spherical and rod nanoparticles (Fig. 3E). Surface potential variation after each reaction was measured by means of DLS confirming the antibody coating in the nanoparticle surface (Fig. 3F).

3.3. Nanoparticle accumulation in static cell culture stimulated by LPS

Following the *in vitro* protocol established previously, endothelial cells were stimulated for 6 h with LPS to induce the VCAM-1 expression and treated with 50 μg (100 μg/mL) during 1, 3 and 6 h. Targeted particles (both in spherical and rod nanoparticles) showed an increased uptake compare to non-targeted in every time point under static cell culture conditions (Fig. 4A). Although no statistical differences were observed, targeted rods showed a higher trend in the accumulation compared to targeted spheres. The difference is more evident when correcting the unspecified accumulation of particles by establishing a ratio between VCAM-1 targeted group and vehicle for both shapes (Fig. 4B) and visualized by confocal microscopy (Fig. 4C and D).

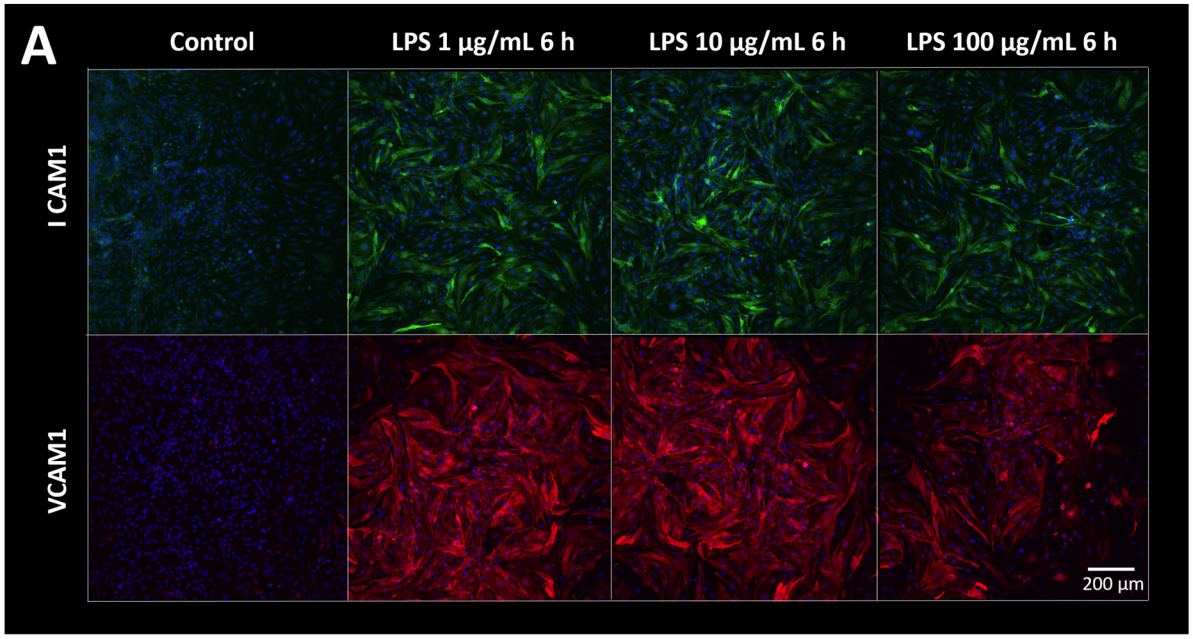

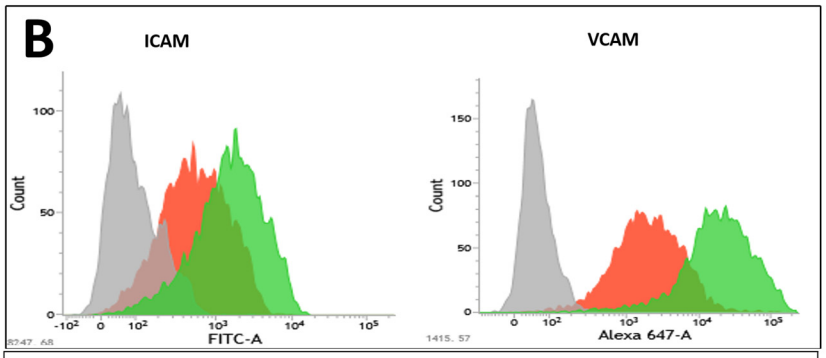

Sample	ICAM1 (AFU)	VCAM1 (AFU)
Blank	85	42
Non-inflamed	576	2029
Inflamed	2476	20826

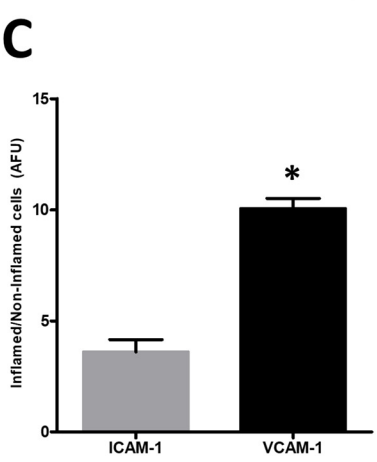

Fig. 1. Analysis of the expression of VCAM-1 and ICAM-1 *in vitro*. (A) Immunofluorescence in bEnd.3 Control cells (without induction of inflammation) and stimulated cells with different concentrations of LPS during 6 h. (B) Cytometric analysis of the expression of ICAM-1 and VCAM-1 in bEnd.3 control endothelial cells and stimulated with LPS for 6 h. Blank group represents cells with no antibody labeling; non-inflamed group represents cells with no inflammation induction but labelled for VCAM-1 or ICAM-1 and inflamed group represents cells with inflammation induction by means of LPS for 6 h and labelled with VCAM-1 or ICAM-1 antibody. Values in the table represents the average of Arbitrary Fluorescent Units (AFU). (C) Fold-increase of the expression of ICAM-1 and VCAM-1 in inflamed cells with respect to the control group. Bars represent SD and * $p < .05$.

3.4. Nanoparticle binding assay under flow conditions in microfluidic devices stimulated by LPS

The effect of nanoparticle shape on particle adhesion under flow was evaluated with microfluidic channels (Fig. 5A) coupled to a microinjection pump to simulate shear stresses (1.00 dyn/cm^2) as would be found *in vivo*. Initially, microfluidic channels were lined with bEnd.3 cells, but to simulate a more translatable human blood brain barrier (BBB) model, hCMEC/D3 cells were used for subsequent experiments (Fig. 5B, Fig. 5C and Supplemental Video 1).

A total of 5×10^{10} nanoparticles/mL of particles were flown for 1 h at 2.35 µL/min. Confocal slices of cell monolayers were analyzed at the bottom of the channel (glass substrate) and the top of the channel (PDMS substrate). Upon comparing particle geometries, no apparent differences were observed between VCAM-1 targeted spheres and non-specific IgG spheres (Fig. 5D and E). Both spherical particles had accumulated similarly in either case. However, more accumulation was observed for VCAM-1 rod particles as compared with the non-specific IgG rods (Fig. 5F), leading to greater targeting efficiency of rod-shaped particles as compared to their spherical counterparts.

3.5. Analysis of nanoparticle biodistribution in animals subjected to LPS-mediated systemic inflammation

Six hours after LPS administration, a dose of 15 mg/kg of nanoparticles was administered i.v. in Swiss mice. After 6 h, the nanoparticle biodistribution was assessed in various organs (brain, kidney, liver, lungs and spleen) by analyzing the emitted radiation. VCAM-1 targeted particles accumulated to a greater extent than the vehicle groups, while no differences in the accumulation were observed between rod and spherical shapes. Higher accumulation was observed in lungs with rod-shaped VACM1 targeted particles. No differences were observed between the four groups tested in the other three organs analyzed (Fig. 6A). Within the brain, no significant differences between shapes

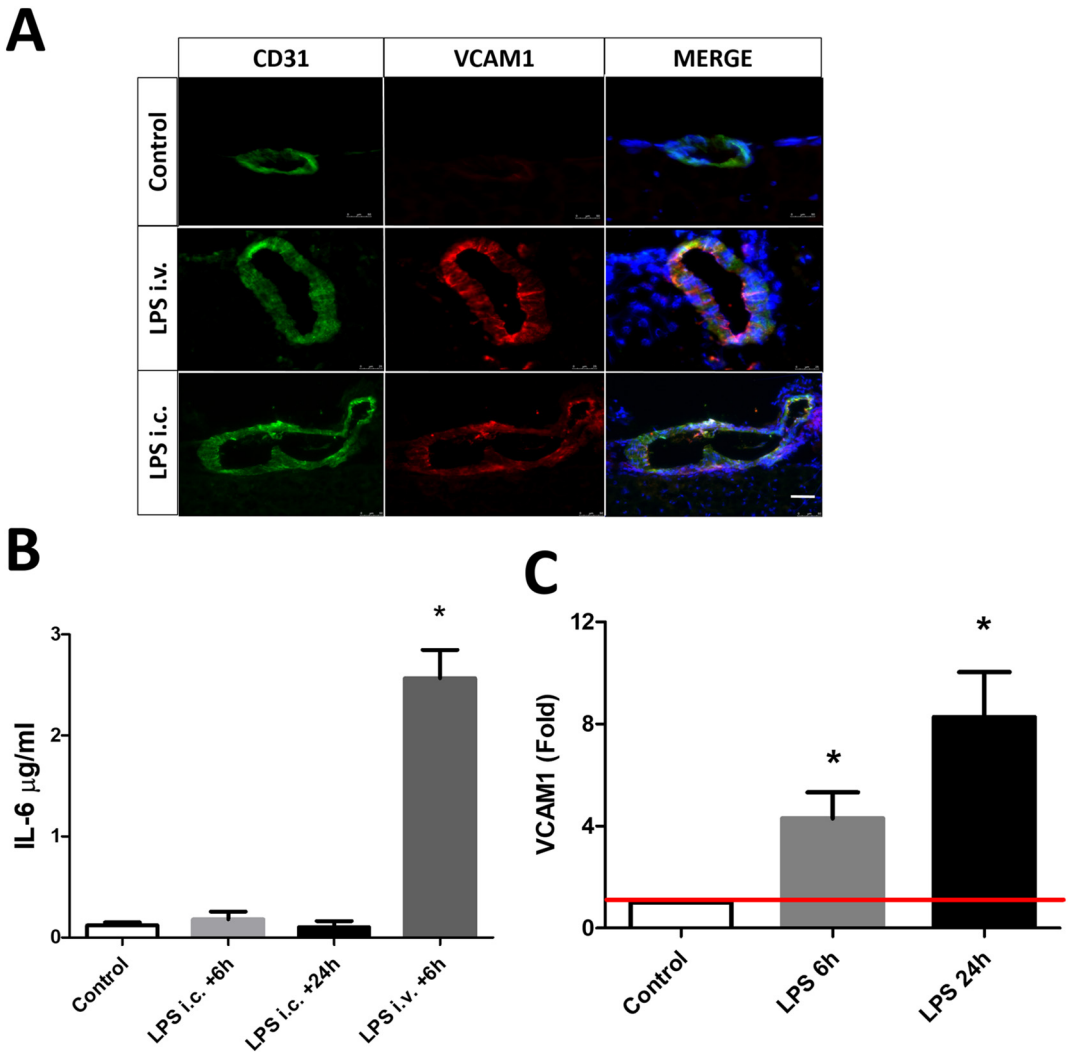

Fig. 2. Inflammatory induction *in vivo* (A) Immunofluorescence staining of CD31 (green), VCAM-1 (Red) and nuclear staining (blue) in 12 µm brain slices of controls and animals treated with LPS intravenous (100 µg/animal) and intracerebral (10 µg/animal). Microphotographs showed were acquired at 20× in vessels, white bar represents 50 µm. (B) IL-6 levels in serum after administered 100 µg of LPS i.v. and i.p. in Swiss mice. (C) Quantification of the relative expression of VCAM1 in the brain of control and inflamed animals by means of qPCR. The red line represents the basal expression of the controls without inflammatory stimulation. Bars represent the average with SD and * $p < .005$ compared with the control group. (For interpretation of the references to colour in this figure legend, the reader is referred to the web version of this article.)

was observed. Spherical particles showed a 1.2-fold increase in accumulation in the targeted group compared to the control, while the rod-shaped particle's accumulation was 1.4-fold compared to the respective control group. The correction by unspecific accumulation establishing the ratio targeted/vehicle shows that only in lung rod-shaped particles presented higher accumulation (Fig. 6B). Raw biodistribution data are included in supplmentary data (supplementary Fig. 1A).

3.6. Nanoparticle brain accumulation in animals subjected to local cerebral inflammation induced by LPS

Previously, we saw an increase in VCAM-1 expression in the brain at 24 h after intracerebral LPS injection. Therefore, a 24 h time point was used for nanoparticles treatment. The dose of nanoparticles was increased to 30 mg/kg (0.9 mg administered in 200 µL) to increase the signal-to-noise ratio. Nanoparticles were administered intravenously 24 h after LPS stimulation. In this cerebral inflammation model, greater accumulation of targeted particles was observed as compared to the respective control groups regardless of the shape, suggesting the increased accumulation was not due to non-specific particle accumulation in the tissue (Fig. 7A). The average ratios between VACM-1 targeted group/vehicle group were analyzed showing that spherical nanoparticles exhibited an uptake 3 times higher in the VCAM-1 group than the control group, while animals treated with rod nanoparticles showed an uptake 3.4 times higher for the VCAM1 group than the control group (Fig. 7B), although the differences between both ratios were not significant. Raw biodistribution data are included in supplmentary data (Supplementary Fig. 1B).

4. Discussion

In this study we performed a longitudinal analysis of the effect of nanoparticle shape on the accumulation in endothelial cells with targeting VCAM-1 markers. Two shapes, polystyrene spheres and polystyrene rods with an aspect ratio of 2 were prepared. Previous literature studies have shown that rod-shaped particles exhibit beneficial attributes in terms of circulation times, biodistribution and cellular uptake [10,23–25]. We first analyzed two endothelial markers as possible targets for the NPs: the adhesion molecules ICAM-1 and VCAM-1 expressed on the luminal side of the endothelial cells. These markers were chosen because of their inducible ability under inflammatory conditions [26], increasing the number of copies expressed in the cell, and

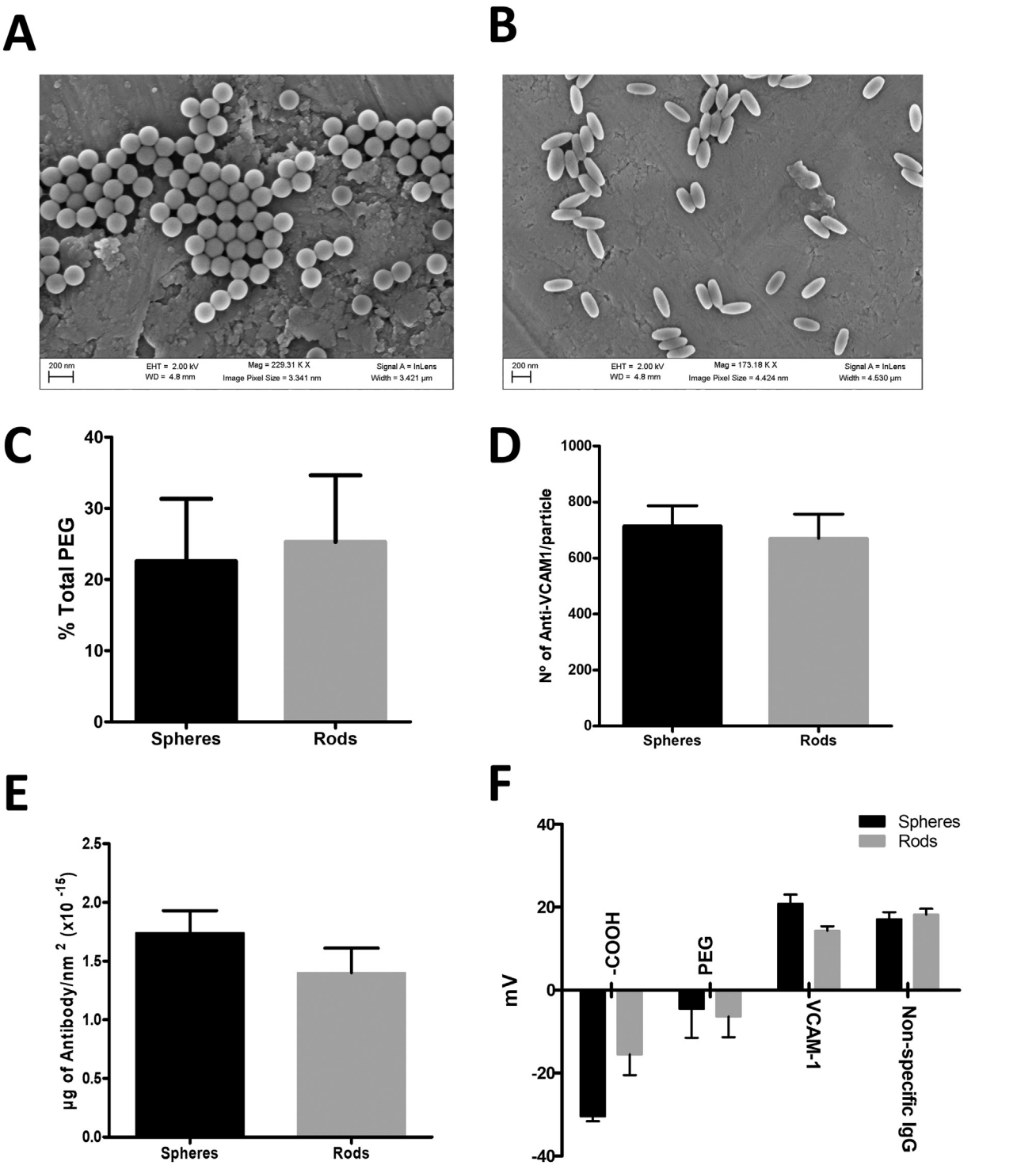

Fig. 3. Nanoparticle characterizations. Scanning electron microscopy (SEM) images of spherical (A) and rod-shaped (B) polystyrene nanoparticles. C) Percentage of PEG incorporated in the particles after the reaction. The values correspond to the average of 5 reactions, bars represent standard deviation. D) Number of anti -VCAM1 antibodies coupled per particle, both in spheres and rods. Graphic show the means and SD of 5 separate antibody coupling reactions. E) VCAM-1 antibody density expressed as µg of antibody per nm^2 for spherical and rod-shaped particles. F) Variation of the zeta potential of spheres and rods after different surface modifications obtained from DLS measurements. The values correspond to the average of 5 reactions. Bars represent average with SD.

increasing the likelihood of binding interactions in pathological tissue and not in the healthy state. Secondly, inflammation is a common occurrence in many neurological diseases such as ischemic and hemorrhagic stroke, Alzheimer's disease, multiple sclerosis, Parkinson's disease, and cancer [26–32]. Vascular inflammatory markers act as a signaling point for circulating immune system cells, taking advantage of this biological mechanism, these proteins can be used as anchors for nanoparticles to treat or diagnose these pathologies more efficiently. Inflammation was induced with LPS of *E. coli*, simulating an infection without the need for the pathogen [33,34]. The expression of the markers was analyzed by means of different methods throughout the study in both *in vitro* and *in vivo* conditions. Initially, the expression of the two markers (ICAM-1 and VCAM-1) was analyzed in cells of the brain microvasculature of mouse (bEnd.3 cells) in a qualitative

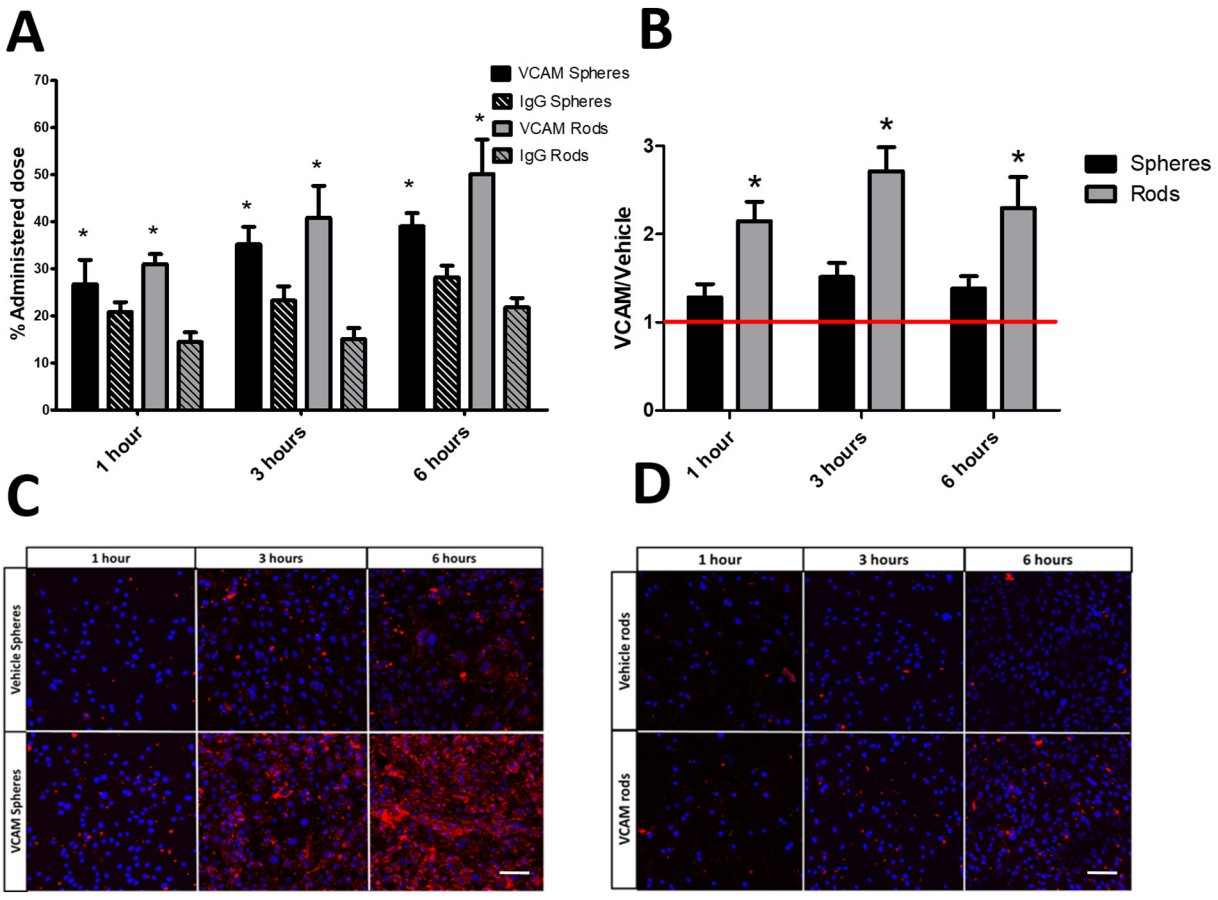

Fig. 4. *In vitro* nanoparticles accumulation in bEnd. 3 endothelial cells. A) Percentage of administered cell dose of vehicle (coated with no specific IgG antibody) and VCAM1 targeted rods and spheres at different time points. B) Accumulation ratio between VCAM1 targeted particles and non-targeted in spheres and rods. Red line represents the accumulation of the vehicle group. Bars represent average with SD and * $p < .005$ compared to the spherical shape. C) Confocal imaging of inflamed Bend.3 endothelial cells nucleus (blue) treated with 50 μg of spherical and D) rod-shaped particles (red) at different time points ($N = 6$ wells/group) after LPS stimulation. Images were acquired at 20× white bars represents 100 μm. (For interpretation of the references to colour in this figure legend, the reader is referred to the web version of this article.)

(immunostaining) and quantitative (flow cytometry) way, demonstrating an increase in the expression of ICAM-1 (4.5-fold increase) and in the VCAM-1 expression (around 10-fold increase) compared to the non-inflamed cells. For this reason, we selected the VCAM-1 for nanoparticle targeting. VCAM-1 was also analyzed *in vivo* (in Swiss male mice) after inflammation induction by qPCR showing a time-dependent expression (8-fold increase after 24 h) and immunostaining (positive for VCAM1 in brain vessels) confirming the overexpression in animal studies.

Polystyrene 200 nm spheres were stretched in one dimension into rods with an aspect ratio of 2, and were functionalized with PEG and antibodies against VCAM-1 endothelial receptor (a non-specific IgG antibody was used as control). Particles targeted to VCAM-1 of each shape were analyzed in comparison with particles coated with a non-specific IgG (defined as control nanoparticles) and tested in different conditions. We first analyzed the shape effect in static cell culture in bEnd.3 cells. Specific spherical particles exhibited a 1.2- to 1.5-fold increase in uptake compared to the control group (IgG-coated spherical particles). Rods exhibited a greater enhancement of 2.1- to 2.5-fold over corresponding controls. The images of confocal microscopy showed a lower fluorescence intensity in the rod shaped-particles, which could give the impression of a smaller accumulation of rods compared to the sphere group. However, this effect is due to the spheres-to-rods stretching process, since there is an important fluorescence bleaching during this procedure and therefore cells incubated with rods showed lower fluorescent intensity despite having the same concentration. Images must be seen only as a reference to visualize the accumulation. In order to make a valid comparison between the two shapes, a normalization according to the administered dose or a ratio with the VCAM/Vehicle group of each shape has been made along the work. These results are in agreement with previous findings that rod-shaped particles not only increase cellular uptake, but also increase specificity of particle-cell interactions [35]. For rods, VCAM-1/control ratio peaked at 3 h which is in agreement with similar studies, further supporting the beneficial rod shape of nanoparticles for targeting cell binding [15,36]. The ability of nanoparticles to adhere to cells and surfaces under flow conditions was tested using microfluidic devices. Microfluidic devices represent a comprehensive strategy to reproduce shear stresses as would be found *in vivo* from the hemodynamic forces. This allows for the induction of changes in endothelial morphology, cytoskeletal remodeling, changes on gene expression, inducing a better endothelial organization and reducing permeability, and mimicking the *in vivo* vascular environment [37]. In this study, microfluidic devices were used to evaluate if shear stress could alter the nanoparticles performance, an approach that is increasingly included in the analysis of nanoparticles where different flow rates are applied to evaluate their effect on different nanostructures to bind to the endothelium [38,39]. Therefore, shear stress is an important parameter to take into account, inversely related to the particle uptake [40]. The greater the shear stress, the lower the probability of adhesion with the lumen target due to the decoupling forces derived from the hydrodynamic forces [38,39]. To perform this study, bEnd.3 and hCMEC/d3 endothelial cells were

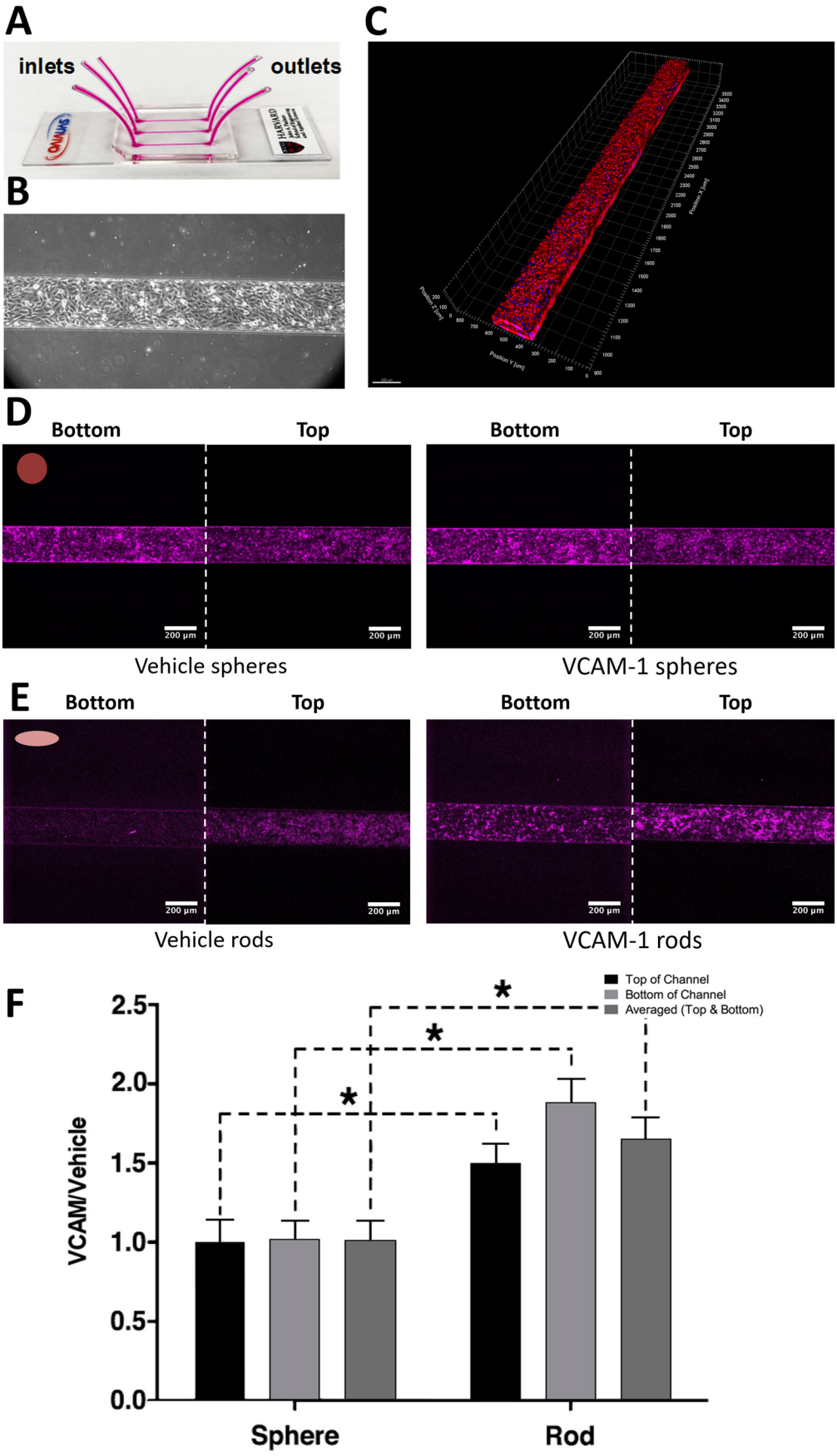

Fig. 5. A) Microfluidic device used to perform the flow assays. B) Bright field image of the central section of a microfluidic chip coated with a monolayer of hCMEC/D3 cells C) Three dimension reconstruction of a section of the microfluidic circuit from images acquired in confocal microscopy. Images acquired by confocal microscopy of top and bottom sections of microfluidic linear circuits after the flow of (D) spherical and (E) rod-shaped nanoparticles. Particles with the same shape were acquired under the same image conditions. F) Accumulation ratio between VCAM targeted particles and non-targeted in spheres and rods. Bars represent the average with SD and * $p < .005$ compared to the spheres group.

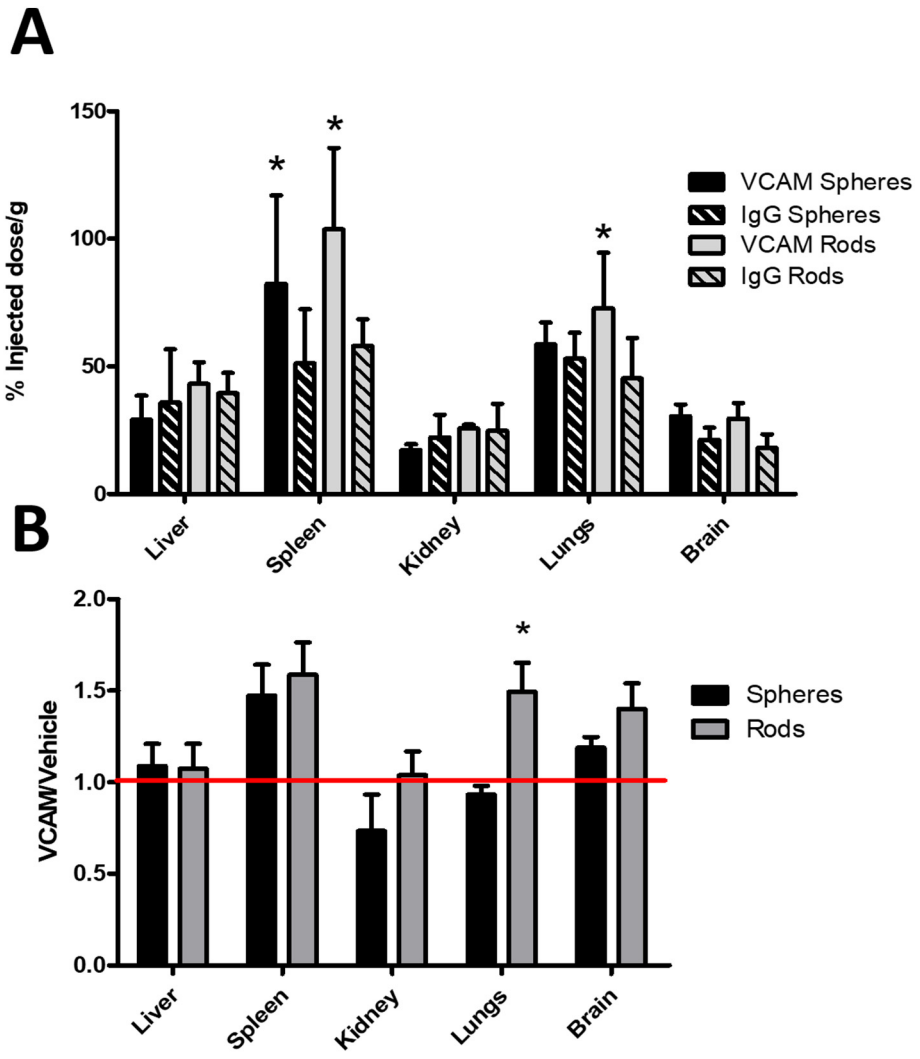

Fig. 6. A) Nanoparticle biodistribution *ex vivo*, in different organs after systemic inflammation induction. * indicates a $p < .05$ compared to vehicle group. B) Ratio between VCAM /IgG media values of % Injected dose/g for spheres and rods. Red line represents the accumulation of the vehicle group. Bars represent the average with SD and * $p < .005$, compared to the spherical shape. (For interpretation of the references to colour in this figure legend, the reader is referred to the web version of this article.)

selected because they represent two of the most used lines in BBB models and brain tissue study as well, since they show a behavior very similar to the microvasculature in physiological and pathological conditions [41–45]. Similar systems have also been used to study nanoparticle penetration into tumors [46].

After flowing the particles for 1 h, no differences were observed in binding of targeted spheres over non-targeted spheres. VCAM-1 rods, on the other hand, exhibited a significant increase in binding under shear stress. Similar studies analyzed the effect of shear stress showing a drastic decrease in cell uptake when applying flow, decreasing proportionally to the shear stress applied to the system [47]. When comparing shapes in static *vs* flow conditions, it can be observed that while under static conditions there are obvious differences between targeted and non-targeted in both shapes; when applying a shear stress of 1 dyn/cm^2, no difference in the uptake of spherical nanoparticles was observed, while the rod targeted group maintained a significant difference compared to the vehicle (1.7-fold increase). These findings suggest rod shapes offer a clear advantage over the spheres in terms of cell binding. Several factors may be responsible for this behavior including better margination of rods, higher surface binding or reduced shear-induced detachment. Indeed, these effects have been studied both in mathematical models and experiments [48,49].

The translation of *in vitro* shape effects to *in vivo* conditions was tested. The behavior of the particles can change significantly under *in vivo* conditions due to different flow conditions, different caliber of vessels and the trapping effect of immunological cells and organs as kidney and liver that reduces the nanoparticles targeting efficacy. In addition, when the nanoparticles are injected in an *in vivo* system, the positive charge due to the antibody functionalization [50,51] leads to electrostatic interactions with negatively charged blood proteins (defined as protein corona) that can mask the targeting ability of nanoparticle in a dose-dependent manner [52] and it can also determine the pathway when reached the cell [53].

Size and shape are important parameters that may determine the composition of the protein corona [54]. To analyze the possible shape effect *in vivo* of sphere and rods, VCAM-1 nanoparticles were injected in systemically inflamed mice. No significant difference in particle accumulation was found in liver, which could be attributed to the entrapment in small vessels or capture for further processing without distinguishing between shapes or targeting. The kidneys contained a low level of accumulation due to the size of this nanoparticles. On the contrary, lungs showed a significant difference between shapes. Only rods and not spheres, exhibited an increase in VCAM-1 group accumulation compared with IgG group, which resembles the results

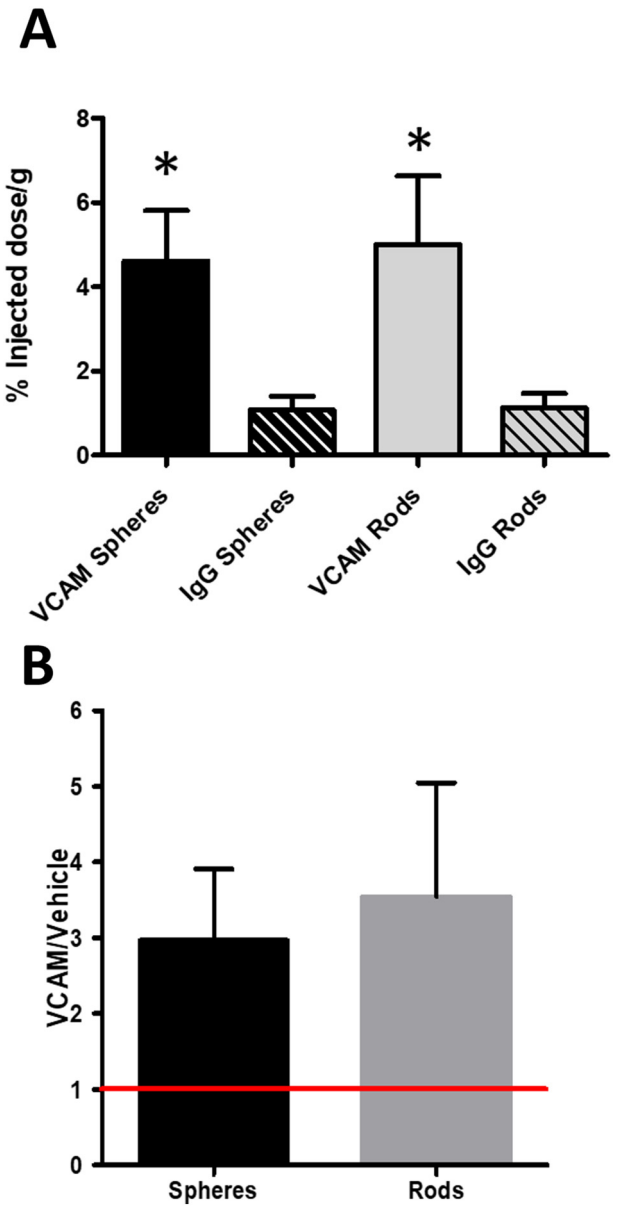

Fig. 7. A) Particle accumulation in brain represented as % of injected dose/mg tissue ($N = 4$ animals/group). Bars represent the average with SD and * $p < .005$ respect to the vehicle group. B) Accumulation ratio between VCAM/IgG media values of % Injected dose/g for spheres and rods. Red line represents the accumulation of the vehicle group. Bars represent the average with SD. (For interpretation of the references to colour in this figure legend, the reader is referred to the web version of this article.)

observed in microfluidic devices. Overall, the lung accumulation of rods and spheres and its dependence on target specificity match well with the results from *in vitro* microfluidic studies. In the brain, targeted spheres as well as rods accumulated better than their non-targeted controls, but the difference was not statistically different. This could have potentially originated from the limitation of the detection or binding of particles to non-analyzed inflamed regions.

In a second approach, we localized the inflammation in the brain by local injection of LPS and observed a significant increase in the accumulation of targeted particles compared to the controls. When comparing the shapes, the rods exhibited a slightly improved the accumulation (3.5-fold) compared to the spheres (3-fold). These results are consistent with the literature reports that elongated shapes exhibit better targeting in the targeted zones compared to the spheres for various materials including polystyrene, silica or iron [13,55,56]. Administration route can also impact the outcome of nanoparticles, Intravenous administration causes a significant loss of particles in off target organs, while an intra-arterial administration of particles can assist in localizing the drug to target organs [57]. The relatively small difference between spheres and rods observed in this study can potentially arise from several factors. First, the aspect ratio of rods used in this study (AR ~2) is much smaller than those used previously (AR~3–4). Hence, the contribution of shape, though clearly seen in *in vitro* experiments, may be masked by the variability of the biological systems. Adsorption of proteins in serum may further reduce the differences in the shapes. Second, the antibody concentration on the surface is lower in rods than in spheres, which may negate some of the contribution of shape-enhanced binding. The stretching process increased the surface area of the particles, but maintained the same number of functional groups for the bioconjugation of the antibody, which leads to a decrease of the surface density of ligands. This could reduce the avidity of the particle for the target, influencing its specific accumulation [58,59]. This study points to the potential existence of a critical lower threshold of aspect ratio which is necessary to bring out the difference between spheres and rods for *in vivo* brain targeting. This issue should be addressed in future studies. Specifically, the nanoparticles with larger aspect ratios should be tested. Additional potential benefits of elongated shapes including increase in the circulation times [60,61] and change in interactions with cells [25,62] and greater penetrance in the target organs especially in tumors [56,63] should be explored in future studies.

5. Conclusions

In this study spherical (200 nm) and rod-shaped (400 nm length) polystyrene particles were used to evaluate the shape effect when targeting VCAM-1 in brain endothelial cells. The results demonstrate accumulation of VCAM-1-targeted rods to the endothelium under static and flow conditions. The inducible nature of the target VCAM-1 under inflammatory conditions limits unspecific accumulation with special importance in neurological diseases with an inflammatory component. Further studies should focus on optimization of parameters, especially of the particle aspect ratio to elicit increased contribution of particle asphericity. Optimization of antibody conjugation to increase surface density should also be performed to increase target specificity. Particles prepared from biocompatible, biodegradable polymers with similar dimensions should also be explored and designed to carry therapeutic payloads. With further optimization, VCAM-1 targeted non-spherical particles could open new therapeutic opportunities.

Supplementary data to this article can be found online at https://doi.org/10.1016/j.jconrel.2019.07.026.

Author contributions

A. D. S—C., performed animal studies and *in vitro* static studies, T.B., performed microfluidic experiments, V.K., participated in the design of nanoparticles, I·P-L., performed the qPCR studies, P.A-G. and A. P-D., helped in the biodistribution studies, A.P. analyzed the flow cytometry data, C·C-P and P.H. helped in the data analysis, J.C. obtained funding for this works S.M. and F.C. designed the research and participated in data analysis and interpretation. All authors contributed to results, discussion, and manuscript writing.

Declaration of Competing Interest

The authors declare no competing financial interests.

Acknowledgements

This study has been partially supported by grants from Instituto de

Salud Carlos III (PI13/00292 and PI17/0054), Spanish Research Network on Cerebrovascular Diseases RETICS-INVICTUS (RD12/0014), Fundación Mutua Madrileña. The Ministry of Economy and Competitiveness of Spain (SAF2017-84267-R). The European Union program FEDER and the European Regional Development Fund – ERDF, MADIA project No. 732678 to FC. Furthermore, F. Campos (CP14/00154) recipients a research contract from Miguel Servet Program of Instituto de Salud Carlos III. National Science Foundation Graduate Research Fellowship under Grant DGE-1745303.

The authors would like to acknowledge the use of Biological Nanostructures Laboratory within the California NanoSystems Institute, supported by the University of California, Santa Barbara and the University of California.

References

[1] W.H. De Jong, P.J. Borm, Drug delivery and nanoparticles:applications and hazards, Int. J. Nanomedicine 3 (2) (2008) 133–149.
[2] S.A.A. Rizvi, A.M. Saleh, Applications of nanoparticle systems in drug delivery technology, Saudi Pharm. J. 26 (1) (2018) 64–70.
[3] S. Gholizadeh, et al., PLGA-PEG nanoparticles for targeted delivery of the mTOR/PI3kinase inhibitor dactolisib to inflamed endothelium, Int. J. Pharm. 548 (2) (2018) 747–758.
[4] K. Jin, et al., Biomimetic nanoparticles for inflammation targeting, Acta Pharm. Sin. B 8 (1) (2018) 23–33.
[5] L.E. Paulis, et al., Targeting of ICAM-1 on vascular endothelium under static and shear stress conditions using a liposomal Gd-based MRI contrast agent, J. Nanobiotechnol. 10 (2012) 25.
[6] R.L. Manthe, S. Muro, ICAM-1-targeted nanocarriers attenuate endothelial release of soluble ICAM-1, an inflammatory regulator, Bioeng. Transl. Med. 2 (1) (2017) 109–119.
[7] R.L. Manthe, S. Muro, ICAM-1-targeted nanocarriers attenuate endothelial release of soluble ICAM-1, an inflammatory regulator, Bioeng. Transl. Med. 2 (1) (2017) 109–119.
[8] M. Gauberti, et al., Ultra-sensitive molecular MRI of vascular cell adhesion molecule-1 reveals a dynamic inflammatory penumbra after strokes, Stroke 44 (7) (2013) 1988–1996.
[9] A. Verma, F. Stellacci, Effect of surface properties on nanoparticle-cell interactions, Small 6 (1) (2010) 12–21.
[10] S. Muro, et al., Control of endothelial targeting and intracellular delivery of therapeutic enzymes by modulating the size and shape of ICAM-1-targeted carriers, Mol. Ther. 16 (8) (2008) 1450–1458.
[11] D. Shenoy, et al., Surface functionalization of gold nanoparticles using hetero-bifunctional poly(ethylene glycol) spacer for intracellular tracking and delivery, Int. J. Nanomedicine 1 (1) (2006) 51–57.
[12] Y. He, K. Park, Effects of the microparticle shape on cellular uptake, Mol. Pharm. 13 (7) (2016) 2164–2171.
[13] P. Kolhar, et al., Using shape effects to target antibody-coated nanoparticles to lung and brain endothelium, Proc. Natl. Acad. Sci. 110 (26) (2013) 10753.
[14] P. Decuzzi, M. Ferrari, The adhesive strength of non-spherical particles mediated by specific interactions, Biomaterials 27 (30) (2006) 5307–5314.
[15] X. Liu, et al., Size dependent cellular uptake of rod-like bionanoparticles with different aspect ratios, Sci. Rep. 6 (2016) 24567.
[16] J.A. Champion, Y.K. Katare, S. Mitragotri, Making polymeric micro- and nanoparticles of complex shapes, Proc. Natl. Acad. Sci. U. S. A. 104 (29) (2007) 11901–11904.
[17] S. Miyazaki, et al., Intraperitoneal injection of lipopolysaccharide induces dynamic migration of Gr-1high polymorphonuclear neutrophils in the murine abdominal cavity, Clin. Diagn. Lab. Immunol. 11 (3) (2004) 452–457.
[18] M. Palermo, et al., Pretreatment of mice with lipopolysaccharide (LPS) or IL-1beta exerts dose-dependent opposite effects on Shiga toxin-2 lethality, Clin. Exp. Immunol. 119 (1) (2000) 77–83.
[19] A.L. Moreira, et al., Thalidomide protects mice against LPS-induced shock, Braz. J. Med. Biol. Res. 30 (10) (1997) 1199–1207.
[20] T. Tanaka, M. Narazaki, T. Kishimoto, IL-6 in inflammation, immunity, and disease, Cold Spring Harb. Perspect. Biol. 6 (10) (2014) a016295.
[21] L.R. Campbell, et al., Intracerebral lipopolysaccharide induces neuroinflammatory change and augmented brain injury in growth-restricted neonatal rats, Pediatr. Res. 71 (6) (2012) 645–652.
[22] C.N. Montero-Menei, et al., Lipopolysaccharide intracerebral administration induces minimal inflammatory reaction in rat brain, Brain Res. 653 (1–2) (1994) 101–111.
[23] J.A. Champion, Y.K. Katare, S. Mitragotri, Particle shape: a new design parameter for micro- and nanoscale drug delivery carriers, J. Control. Release 121 (1–2) (2007) 3–9.
[24] S. Venkataraman, et al., The effects of polymeric nanostructure shape on drug delivery, Adv. Drug Deliv. Rev. 63 (14–15) (2011) 1228–1246.
[25] N. Doshi, S. Mitragotri, Macrophages recognize size and shape of their targets, PLoS One 5 (4) (2010) e10051.
[26] C.W. Smith, Endothelial adhesion molecules and their role in inflammation, Can. J. Physiol. Pharmacol. 71 (1) (1993) 76–87.
[27] F. Pérez-Cerdá, M.V. Sánchez-Gómez, C. Matute, The link of inflammation and neurodegeneration in progressive multiple sclerosis, Mult. Scler. Demyelinating Disord. 1 (1) (2016) 9.
[28] E. Lyros, et al., Molecular links between endothelial dysfunction and neurodegeneration in Alzheimer's disease, Curr. Alzheimer Res. 11 (1) (2014) 18–26.
[29] T. Wyss-Coray, J. Rogers, Inflammation in Alzheimer disease-a brief review of the basic science and clinical literature, Cold Spring Harb. Perspect. Med. 2 (1) (2012) a006346.
[30] S. Amor, et al., Inflammation in neurodegenerative diseases–an update, Immunology 142 (2) (2014) 151–166.
[31] G. Bomboi, et al., Alzheimer's disease and endothelial dysfunction, Neurol. Sci. 31 (1) (2010) 1–8.
[32] F. Cosentino, et al., Endothelial dysfunction and stroke, J. Cardiovasc. Pharmacol. 38 (Suppl. 2) (2001) S75–S78.
[33] O. Lykhmus, et al., Molecular mechanisms regulating LPS-induced inflammation in the brain, Front. Mol. Neurosci. 9 (2016) 19.
[34] H. Fang, et al., Lipopolysaccharide-induced macrophage inflammatory response is regulated by SHIP, J. Immunol. 173 (1) (2004) 360–366.
[35] S. Barua, et al., Particle shape enhances specificity of antibody-displaying nanoparticles, Proc. Natl. Acad. Sci. 110 (9) (2013) 3270.
[36] P. Kolhar, et al., Using shape effects to target antibody-coated nanoparticles to lung and brain endothelium, Proc. Natl. Acad. Sci. U. S. A. 110 (26) (2013) 10753–10758.
[37] C.F. Buchanan, et al., Flow shear stress regulates endothelial barrier function and expression of angiogenic factors in a 3D microfluidic tumor vascular model, Cell Adhes. Migr. 8 (5) (2014) 517–524.
[38] J. Kusunose, et al., Microfluidic system for facilitated quantification of nanoparticle accumulation to cells under laminar flow, Ann. Biomed. Eng. 41 (1) (2013) 89–99.
[39] K. Khodabandehlou, et al., Targeting cell adhesion molecules with nanoparticles using in vivo and flow-based in vitro models of atherosclerosis, Exp. Biol. Med. (Maywood) 242 (8) (2017) 799–812.
[40] M.J. Gomez-Garcia, et al., Nanoparticle localization in blood vessels: dependence on fluid shear stress, flow disturbances, and flow-induced changes in endothelial physiology, Nanoscale 10 (32) (2018) 15249–15261.
[41] T. Masuda, et al., Large-scale quantitative comparison of plasma transmembrane proteins between two human blood-brain barrier model cell lines, hCMEC/D3 and HBMEC/cibeta, Mol. Pharm. 16 (5) (2019) 2162–2171.
[42] A.E. Toth, et al., The endo-lysosomal system of bEnd.3 and hCMEC/D3 brain endothelial cells, Fluids Barriers CNS 16 (1) (2019) 14.
[43] T.D. Brown, et al., A microfluidic model of human brain (μHuB) for assessment of blood brain barrier, Bioeng. Transl. Med. 4 (2) (2019) e10126.
[44] T. Watanabe, et al., Paracellular barrier and tight junction protein expression in the immortalized brain endothelial cell lines bEND.3, bEND.5 and mouse brain endothelial cell 4, Biol. Pharm. Bull. 36 (3) (2013) 492–495.
[45] F. He, et al., Immortalized mouse brain endothelial cell line Bend.3 displays the comparative barrier characteristics as the primary brain microvascular endothelial cells, Zhongguo Dang Dai Er Ke Za Zhi 12 (6) (2010) 474–478.
[46] M. Jarvis, et al., Microfluidic co-culture devices to assess penetration of nanoparticles into cancer cell mass, Bioeng. Transl. Med. 2 (3) (2017) 268–277.
[47] A. Lin, et al., Shear-regulated uptake of nanoparticles by endothelial cells and development of endothelial-targeting nanoparticles, J. Biomed. Mater. Res. A 93 (3) (2010) 833–842.
[48] J. Tan, et al., The influence of size, shape and vessel geometry on nanoparticle distribution, Microfluid. Nanofluid. 14 (1–2) (2013) 77–87.
[49] J. Liu, et al., Computational model for nanocarrier binding to endothelium validated using in vivo, in vitro, and atomic force microscopy experiments, Proc. Natl. Acad. Sci. U. S. A. 107 (38) (2010) 16530–16535.
[50] S. Tenzer, et al., Rapid formation of plasma protein corona critically affects nanoparticle pathophysiology, Nat. Nanotechnol. 8 (10) (2013) 772–781.
[51] M.P. Monopoli, et al., Biomolecular coronas provide the biological identity of nanosized materials, Nat. Nanotechnol. 7 (12) (2012) 779–786.
[52] M. Merhi, et al., Study of serum interaction with a cationic nanoparticle: implications for in vitro endocytosis, cytotoxicity and genotoxicity, Int. J. Pharm. 423 (1) (2012) 37–44.
[53] Y. Yan, et al., Differential roles of the protein corona in the cellular uptake of nanoporous polymer particles by monocyte and macrophage cell lines, ACS Nano 7 (12) (2013) 10960–10970.
[54] N.B. Shah, et al., Blood-nanoparticle interactions and in vivo biodistribution: impact of surface PEG and ligand properties, Mol. Pharm. 9 (8) (2012) 2146–2155.
[55] X. Huang, et al., The shape effect of Mesoporous silica nanoparticles on biodistribution, clearance, and biocompatibility in vivo, ACS Nano 5 (7) (2011) 5390–5399.
[56] J.H. Park, et al., Magnetic Iron oxide nanoworms for tumor targeting and imaging, Adv. Mater. 20 (9) (2008) 1630–1635.
[57] O.A. Marcos-Contreras, et al., Combining vascular targeting and the local first pass provides 100-fold higher uptake of ICAM-1-targeted vs untargeted nanocarriers in the inflamed brain, J. Control. Release 301 (2019) 54–61.
[58] B.J. Zern, et al., Reduction of nanoparticle avidity enhances the selectivity of vascular targeting and PET detection of pulmonary inflammation, ACS Nano 7 (3) (2013) 2461–2469.
[59] S. Wang, E.E. Dormidontova, Nanoparticle design optimization for enhanced targeting: Monte Carlo simulations, Biomacromolecules 11 (7) (2010) 1785–1795.
[60] V.V. Shuvaev, et al., Endothelial targeting of antibody-decorated polymeric filomicelles, ACS Nano 5 (9) (2011) 6991–6999.
[61] Y. Geng, et al., Shape effects of filaments versus spherical particles in flow and drug delivery, Nat. Nanotechnol. 2 (4) (2007) 249–255.
[62] J.A. Champion, S. Mitragotri, Role of target geometry in phagocytosis, Proc. Natl. Acad. Sci. U. S. A. 103 (13) (2006) 4930.
[63] V.P. Chauhan, et al., Fluorescent nanorods and nanospheres for real-time in vivo probing of nanoparticle shape-dependent tumor penetration, Angew. Chem. Int. Ed. Eng. 50 (48) (2011) 11417–11420.